

## Article

# Microstructure and Properties of Al-Cu-Fe-Ce Quasicrystalline-Reinforced 6061 Aluminum Matrix Composites after Aging

Juan Wang <sup>1,2</sup> , Yanhu He <sup>1,\*</sup> and Zhong Yang <sup>2,\*</sup>

<sup>1</sup> College of Intelligent Manufacturing and Elevator Technology, Huzhou Vocational & Technical College, Huzhou 313000, China; 15147478948@163.com

<sup>2</sup> School of Materials and Chemical Engineering, Xi'an Technological University, Xi'an 710021, China

\* Correspondence: heyhanhu6352@126.com (Y.H.); yz750925@163.com (Z.Y.)

**Abstract:** Al-Cu-Fe-Ce quasicrystalline-reinforced 6061 aluminum matrix composites were prepared through hot press sintering and treated with a solid solution and aging treatments. The influence of the solid solution and aging treatments on the microstructure and mechanical properties of the composites was investigated by XRD, EDS, SEM, and TEM. The results show that using Al-Cu-Fe-Ce quasicrystalline intermediate alloy as the reinforcing phase increases the interfacial areas of the composites and enhances the grain boundary strengthening effect, which is conducive to the improvement of the mechanical properties of the composites. And through the solid solution and aging treatment, the  $\beta$  phase and the  $\text{Al}_2\text{CuMg}$  phase belonging to the orthorhombic crystal system, as well as the  $\beta''$  phase and a small amount of the  $\beta'$  precipitated phase, were formed in aluminum matrix composites, and these precipitated phases all existed in the composites in a fine and uniform distribution, which ensured the consistency of the mechanical properties of the materials and improved the mechanical properties of the composites. Meanwhile, the deficiency of quasicrystalline particle-reinforced 6061 aluminum matrix composites in age-hardening was solved and the age-hardening capability of the composites was further developed. This method provides a feasible process route for the preparation of high-performance aluminum matrix composites. The application of this process is expected to improve the mechanical properties and durability of this composite and offer a more reliable option for the application of aluminum matrix composites in aerospace, transportation, and other fields.

**Keywords:** composites; aging treatment; precipitated phase; mechanical properties



**Citation:** Wang, J.; He, Y.; Yang, Z. Microstructure and Properties of Al-Cu-Fe-Ce Quasicrystalline-Reinforced 6061 Aluminum Matrix Composites after Aging. *Coatings* **2024**, *14*, 372. <https://doi.org/10.3390/coatings14030372>

Academic Editor: Andrea Nobili

Received: 4 March 2024

Revised: 17 March 2024

Accepted: 20 March 2024

Published: 21 March 2024



**Copyright:** © 2024 by the authors. Licensee MDPI, Basel, Switzerland. This article is an open access article distributed under the terms and conditions of the Creative Commons Attribution (CC BY) license (<https://creativecommons.org/licenses/by/4.0/>).

## 1. Introduction

Al-Mg-Si series (6000 series) aluminum alloys are widely used in aerospace, transportation, automotive, construction, electronic devices, etc. [1,2]. They have excellent strength, modulus of elasticity, fatigue resistance, as well as good corrosion resistance and forming properties [3,4].

In order to further improve their mechanical properties, particle-reinforced 6061 aluminum matrix composites are usually prepared by adding some reinforcing phases [5,6]. However, incorporating these reinforcing particles can present some challenges [7]. One of the main problems involves the non-uniform distribution of particles, which leads to large differences in the crystal structures and properties in localized areas. The bonding of the reinforcing particles to the aluminum matrix is not tight and is prone to spalling or loosening, especially for certain reinforcing particles that need to be pre-treated, or else the overall performance of the composite will be affected. In addition, some of the particles will react with the aluminum base material to form a new phase structure, leading to changes in the microstructure and properties. And at high temperatures, some particles

may melt or coalesce, resulting in an unstable microstructure and reduced properties of the composite material.

Combined with related literature [8–11], it can be seen that some quasicrystalline intermediate alloys are often added as reinforcing phases to solve the above problems. This is because, among the many particle-reinforced aluminum matrix composites, the quasicrystalline particle-reinforced aluminum matrix composites have unique advantages [11–13]. Firstly, during the process of preparing the composites, because quasicrystals have a certain metal crystal structure (that is, quasi-periodic translational ordering), the quasicrystalline particles can be wetted with the metal liquid [10,14,15], so as to prevent other reinforcers from not being wetted with the metal liquid or from reacting with the matrix metal to produce an undesirable interface [16,17]. Furthermore, the quasicrystalline particles can continue to combine with the base metal to form intermediate alloys that can be utilized twice. Therefore, the research and application of quasicrystalline-reinforced aluminum matrix composites are conducive to energy saving and emission reduction, and promote the concept of green and ecological development.

On this basis, in order to further improve the microstructure of the composites and enhance the mechanical properties of the composites, combined with the characteristics of 6061 aluminum matrix composites, the aging treatment process has an important influence on the microstructure and properties of quasicrystalline-reinforced 6061 aluminum matrix composites [16,18,19]. Reasonable control of aging treatment parameters (e.g., temperature, time, etc.) can realize the uniform solid solution and phase transformation of particles and, thus, improve the mechanical properties of materials [20,21]. Therefore, this study systematically investigates the effect of the solid solution aging treatment on the microstructure and properties of quasicrystalline-reinforced 6061 aluminum matrix composites, aiming to provide certain theoretical guidance for their industrialized and stable production.

## 2. Experimental

### 2.1. Characterization of the Matrix and Reinforcing Materials

Utilizing a vacuum arc melting furnace, the formation of the quasicrystal master alloy, designated as  $(Al_{63}Cu_{25}Fe_{12})_{99}Ce_1$  (in atomic percentage) or 1Ce-IQC, was accomplished. A subsequent thermal process yielded an alloy consisting predominantly of the I phase, alongside a minor presence of the  $Al_{13}Ce_2Cu_{13}$  phase. Detailed methodologies for the synthesis and thermal processing of the I phase have been expounded upon in earlier scholarly works [13,22]. Figure 1 shows the microstructure morphology of 1Ce-IQC reinforcement with average particle sizes of 120  $\mu m$  and 60  $\mu m$ , respectively. It can be seen that the particles exhibit an irregular polyhedral shape, and this shape makes the particles produce different thermal stress fields in different directions, which reduces the coefficient of thermal expansion for both the matrix as well as the composite material to a certain extent.

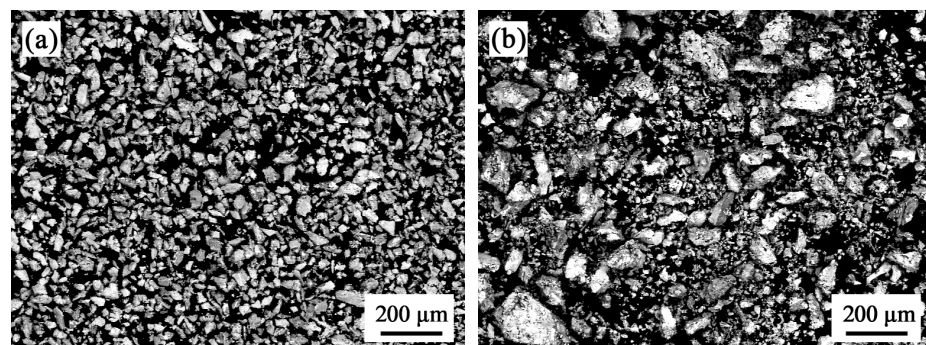


**Figure 1.** Microstructure morphology of 1Ce-IQC particles with different particle sizes after grinding: (a) 60  $\mu m$ ; (b) 120  $\mu m$ .

The 6061 aluminum powder predominantly possesses particle sizes of around 35  $\mu\text{m}$ ; however, a fraction of finer particles measuring approximately 5  $\mu\text{m}$  is also present. The coexistence of these larger and smaller particles plays a significant role in enhancing the composite's thermal expansion characteristics. Combined with relevant literature [11], the specific chemical makeup of the 6061 powder is detailed in Table 1. Images captured through scanning electron microscopy (SEM) of the 6061 aluminum powder's morphology are presented in Figure 2a–d, depicting a spherical geometry. Apart from aluminum, the 6061 powder contains minute quantities of both silicon and magnesium.

**Table 1.** Chemical composition of 6061 material/wt% [11].

Powders	Fe	Si	Mg	Cu	Mn	Cr	Zn	Ti	Al
6061	0.157	0.56	0.81	0.166	0.071	0.051	0.031	0.002	Residuals

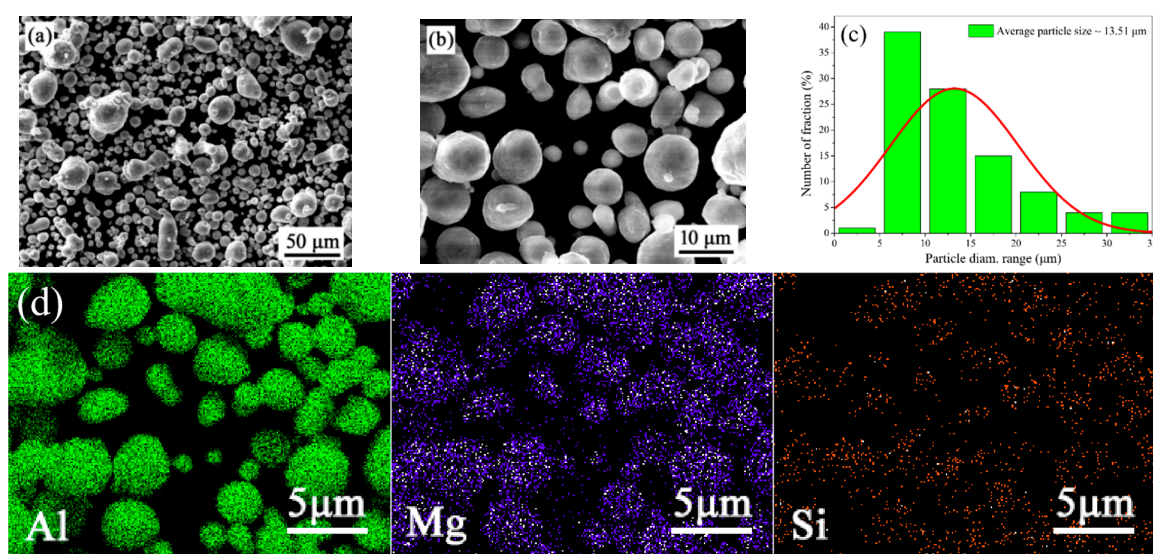


**Figure 2.** Morphology and particle size distribution of 6061 aluminum alloy powder [11]: (a,b) powder morphology; (c) particle size distribution; (d) corresponding to the distribution of Al, Mg, and Si elements in (b).

## 2.2. Preparation and Characterization of Composite Materials

Quasicrystal-strengthened 6061 aluminum matrix composites (6061-20IQC) were synthesized utilizing a ZT-40-20Y vacuum hot pressing furnace (Suzhou, China), wherein the pre-prepared reinforcement phase was amalgamated with the matrix material at a volumetric ratio of 20:80. The homogeneously blended powders were consolidated within graphite die with an approximate diameter of 30 mm, undergoing sintering in a  $10^{-3}$  Pa vacuum pressure environment with a compaction force of 30 MPa throughout the hot pressing sintering sequence. To discern the influence of sintering parameters on the resultant composite, the hot press sintering process was executed at varying temperatures (470  $^{\circ}\text{C}$ , 490  $^{\circ}\text{C}$ , and 510  $^{\circ}\text{C}$ ) and durations (10 min, 20 min, 30 min, and 40 min).

Combined with previous studies [11], the optimal hot press sintering process was 490  $^{\circ}\text{C}$  with a holding time of 30 min. Therefore, the composite was subjected to a solid solution plus aging treatment with a view of further improving the microstructure and strengthening the mechanical properties of the composite.

Combined with the characteristics of 6061 aluminum alloy composites [23], the solid solution heat treatment process involves heating to 530  $^{\circ}\text{C}$ , preserving for 1 h, followed by water cooling. Meanwhile, 6061 aluminum powder belongs to the Al-Mg-Si system alloy, which has four precipitation phases during aging, namely, the GP zone,  $\beta''$ ,  $\beta'$ , and  $\beta$  phase, among which, the  $\beta''$  phase is the key precipitation phase causing the aging strengthening

of Al-Mg-Si alloy [24–26]. However, the  $\beta''$  phase precipitation process is slow when aging is carried out below 150 °C. Therefore, combined with the related literature [24], this paper uses 170 °C as the aging temperature, and the aging times are 2 h, 4 h, 6 h, 8 h, 10 h, 12 h, 16 h, 20 h, and 24 h, respectively, to study the effect of aging time on the properties of the composites, and to provide a reference for the formulation of the heat treatment process for industrial production.

Employing X-ray diffraction (XRD-6000, Shimadzu, Kyoto, Japan) with Cu- $K_{\alpha}$  emission (wavelength of 0.1542 nm), an anode potential of 40 kV, and an electron stream of 30 mA, at a sweep velocity of 4 degrees per minute over a Bragg angle range of  $2\theta = 20^{\circ}$  to  $90^{\circ}$ , we explored the crystalline phases precipitated in the alloys synthesized through the application of the hot pressing method. To scrutinize the microstructural attributes of the alloys, we resorted to scanning electron microscopy (SEM, TESCAN, VEGA II-XMU), augmented with energy-dispersive spectroscopy (EDS), and delved into finer details via transmission electron microscopy (TEM < FEI Talos F200X). To ascertain and adjust the interplanar distances within the crystals, our methodology included the utilization of Digital Micrography software (Version 3.22.1461.0).

The HM-211 Vickers microhardness tester was used to test the hardness of the composites prepared by different aging processes. A wire cutter was used to cut out the square specimens measuring  $8 \times 8 \times 8$  mm, and the specimens were polished and sanded one by one to ensure that the surfaces of the specimens were clean and smooth. The hardness test parameters were set to a 150 g load, a 15 s holding time, and 10 points for each sample, and the average value was taken as the final Vickers hardness value of the specimen.

The room temperature tensile properties of the quasicrystalline particle-reinforced aluminum matrix composites were tested using a CMT5105 universal tensile testing machine with a tensile rate of 1 mm/min. For each condition, three specimens were cut and processed into thin slices, and their sizes and shapes are shown in Figure 3. The samples were polished with sandpaper to reduce the stress concentration, and the tensile tests were performed and averaged.

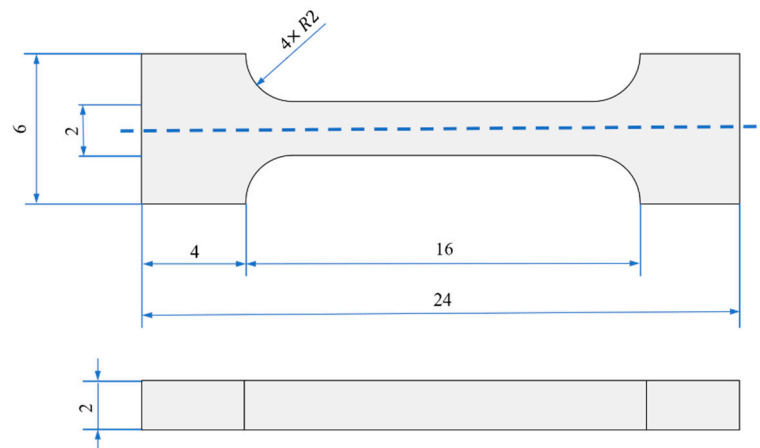


**Figure 3.** Size and shape of tensile specimen.

### 3. Results

#### 3.1. Effect of Aging Time on the Microstructure of 1Ce-IQCp/6061

Based on the previous analysis [11], the optimal hot pressing process is 490 °C for 30 min, and the microstructure of the 1Ce-IQCp/6061 composites prepared under the optimal hot pressing process is shown in Figure 4.

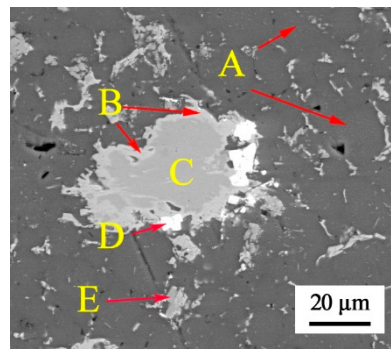


**Figure 4.** Microstructure of the sintered 1Ce-IQCp/6061 held at 490 °C for 30 min.

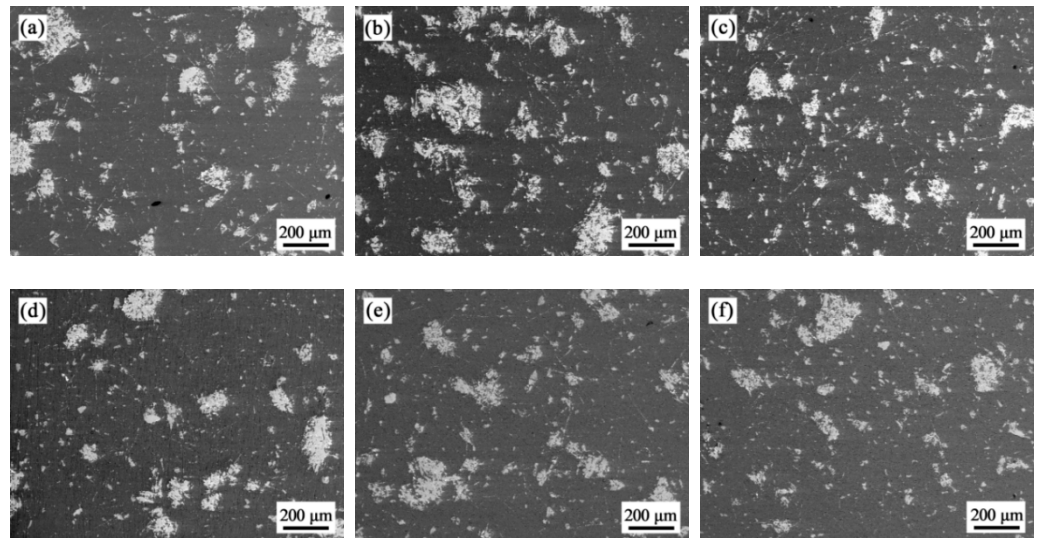
Combined with the energy spectrum analysis (Table 2), it can be seen that there are five regions, A, B, C, D, and E. The A region is the aluminum matrix; the B region is the transition layer formed by the reaction between the quasicrystal and matrix, which is mainly composed of  $\text{Al}_7\text{Cu}_2\text{Fe}$ ; combined with the previous analysis [11], the use of Al-Cu-Fe-Ce quasicrystalline intermediate alloy as the reinforcing phase increases the interfacial area of the 1Ce-IQCp/6061 composites. Moreover, the grain boundary reinforcement effect is better, which is conducive to improving the mechanical properties of the 1Ce-IQCp/6061 composites. The C region is the I phase, and there is no porosity or holes appearing in this region; the white D region, immediately adjacent to the C region, is the  $\text{Al}_{13}\text{Ce}_2\text{Cu}_{13}$  phase, which is closely connected to the quasicrystalline phase and is always present from the beginning of the preparation of the as-cast quasicrystalline intermediate alloys to the preparation of 1Ce-IQCp/6061, which suggests that the phase has good thermal stability.

**Table 2.** EDS point-scan analysis of each forming phase in 1Ce-IQCp/6061 sintered at 490 °C for 30 min.

Hot Pressing Sintering Temperature	Area	Al		Fe		Cu		Ce		Corresponding Phase
		wt%	at%	wt%	at%	wt%	at%	wt%	at%	
490 °C	A	97.29	98.83			2.71	1.17			Al matrix
	B	53.83	72.44	15.04	9.78	31.12	17.78			$\omega$ -phase
	C	36.7	63.52	2.05	1.72	35.72	26.26	25.52	8.51	I phase
	D	24.19	46.3	6.98	6.4	51.33	41.88	17.5	5.42	$\text{Al}_{13}\text{Ce}_2\text{Cu}_{13}$ -phase
	E	31.96	49.56	63.19	47.24	4.85	3.2			$\beta$ - $\text{Al}_5(\text{Cu,Fe})_5$ -phase

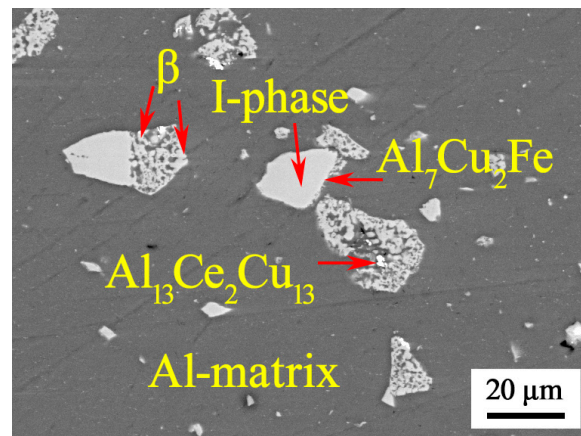
Zone E is composed of the  $\beta$  phase, which may be the residual phase left from the heat treatment of the cast alloy or could be formed through a reaction between the quasicrystalline phase and the matrix during subsequent hot pressing. When the hot pressing temperature exceeds 490 °C, or when the material is kept at elevated temperatures for an extended period of time, there will be mutual diffusion between the reinforcement and the matrix, leading to gradual decomposition within the reinforcement.

Figure 5 shows the microstructure and morphology of 1Ce-IQCp/6061 after different aging times at 170 °C. The large white particles in Figure 5 represent the retained reinforcement after aging, and the small white particles are distributed along the grain boundaries, which are identified as the precipitated phase after aging. With the increase in the aging holding time, the number of small particles precipitated along the grain boundaries of the matrix increases, especially after aging for 10 h, when the number of these small particles increases significantly.



**Figure 5.** Microstructure of 1Ce-IQCp/6061 at different aging holding times: (a) 2 h; (b) 4 h; (c) 6 h; (d) 8 h; (e) 10 h; and (f) 12 h.

However, a common characteristic of the aging of 1Ce-IQCp/6061 composite materials is that the large white particles in the reinforcement have undergone obvious diffusion. Taking the microstructure of the composite material after 10 h of aging as an example, as shown in Figure 6, it can be seen that there is obvious diffusion around the large white particles. The reason is that, according to the previous analysis, the optimal hot pressing process is 490 °C. When this temperature is exceeded, mutual diffusion occurs between the reinforcement and the matrix, leading to the gradual decomposition of the reinforcement. The main phase formed after the decomposition of the large particles is the  $\beta$  phase.



**Figure 6.** Microstructure of 1Ce-IQCp/6061 after aging time of 10 h.

TEM observations of 1Ce-IQCp/6061 specimens after aging for 10 h were performed to determine the phases of small white particles precipitated along grain boundaries, which are diffusely distributed in Figure 7. For some smaller regions, phase determination was performed in conjunction with high-resolution morphology.

Figure 7 shows the TEM characterization of the  $\beta$  phase ( $\text{Al}_{0.5}\text{Fe}_{0.5}$ ) of 1Ce-IQCp/6061 composites after aging for 10 h. As shown in Figure 7, the specimen was held at 170 °C for 10 h after aging, which resulted in a lot of regular particles. The energy spectrum analysis was carried out, as shown in Figure 7; these particles mainly contained aluminum, iron, and some silicon elements, which were determined as the  $\beta$  phase through selected area electron diffraction pattern calibration. Combined with relevant literature, it can be seen [20] that the  $\beta$  phase usually contains only two elements (aluminum and iron), but

after combining with the matrix for hot pressing and sintering, a small amount of silicon in the matrix diffuses into the reinforcing body to form the  $\beta$  phase containing silicon, which still exists after aging, is finely dispersed and uniformly distributed, and plays a very good role in promoting the reinforcement of the 1Ce-IQCp/6061 composites.

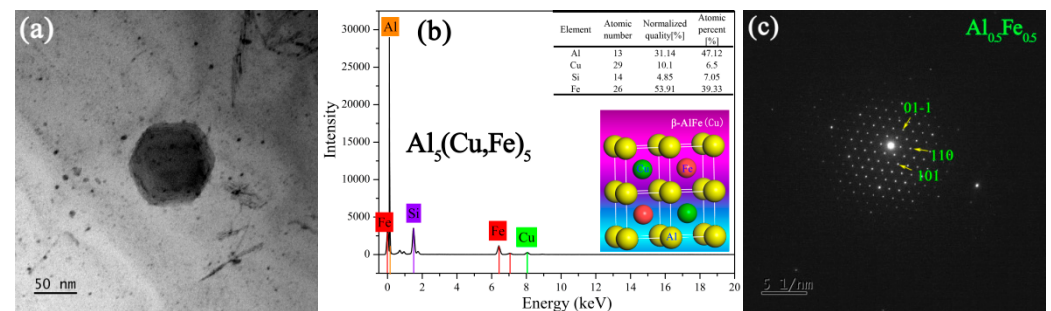


**Figure 7.** TEM characterization of the  $\beta$  phase of 1Ce-IQCp/6061 after 10 h of aging. (a) Bright-field image; (b) energy spectrum analysis of the  $\beta$  phase; (c) microzone diffraction pattern.

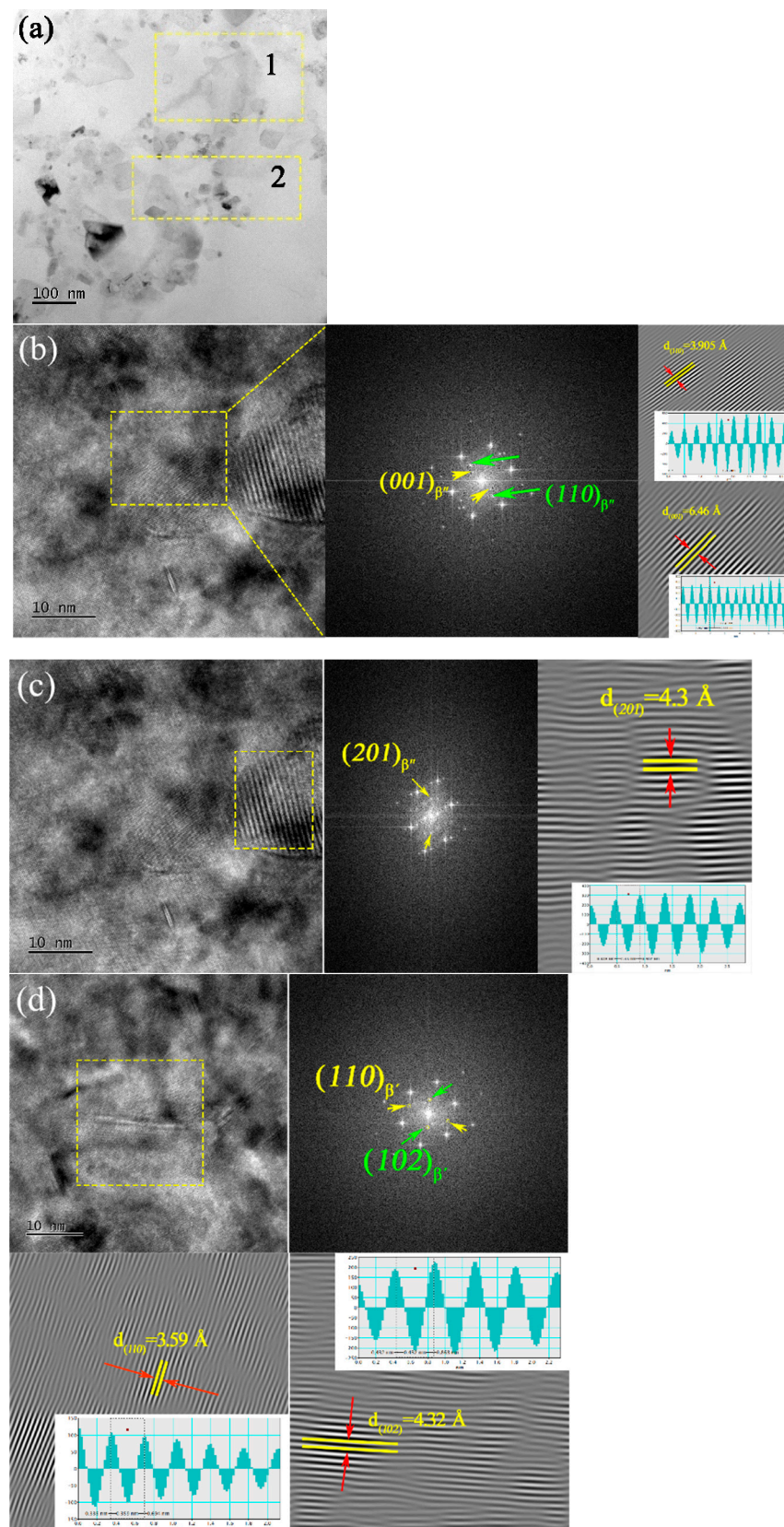
Figure 8 presents the TEM characterization of the 1Ce-IQCp/6061 composite after 10 h of aging. Considering the significant correlation between the aging precipitates and the aluminum matrix, the Al-Mg-Si alloy was observed through TEM along the [001]Al direction. In Figure 8a, the bright-field image of the 1Ce-IQCp/6061 composite after aging reveals a fine and dispersed distribution of precipitates.

Figure 8b,c show the high-resolution morphology and Fourier transform (FFT) of the bright-field image of Figure 8a, the '1' region. The high-resolution morphology (yellow dashed box) shows that the atoms of the precipitated phase are arranged in a regular manner, and the FFT and the calibration of the diffraction spots determine that this region is a  $\beta''$  phase with the chemical composition of  $\text{Mg}_5\text{Si}_6$  ( $a = 1.516$  nm,  $b = 0.405$  nm,  $c = 0.674$  nm), which belongs to a monoclinic crystal system with a monoclinic angle close to  $105.3^\circ$ . Among all the precipitated phases, the  $\beta''$  phase exhibits high co-grid strain energy with the matrix and is the most effective strengthening phase, which can significantly improve the strength and hardness of the composites.

Figure 8d displays the high-resolution microstructure and FFT of region 2 in Figure 8a corresponding to the bright-field image. The high-resolution microstructure reveals that this region consists of elongated needle-shaped precipitates. Performing FFT on Figure 8d indicates that the phase in this region is a  $\beta'$  phase with a chemical formula of  $\text{Mg}_{1.8}\text{Si}$ , belonging to the hexagonal crystal structure ( $a = 0.715$  nm,  $c = 1.215$  nm). Thus, the precipitation sequence of the precipitates in the 1Ce-IQCp/6061 composite after 10 h of aging at  $170^\circ\text{C}$  is as follows:  $\beta''$  phase ( $\text{Mg}_5\text{Si}_6$ )  $\rightarrow$   $\beta'$  phase ( $\text{Mg}_{1.8}\text{Si}$ ).

Regarding the 1Ce-IQCp/6061 composite after aging treatment, there are some regions where there are uniformly distributed white particles, as shown in Figure 9. In order to determine the phase structure of these particles, they were analyzed by a selected electron diffraction pattern; the results are shown in Figure 9. Based on the calibration of the diffraction pattern, it was determined to be the  $\text{Al}_2\text{CuMg}$  phase, which belongs to the orthorhombic crystal system. The observation of the facet element distribution in this region was carried out; the results are shown in Figure 10. It can be seen that the white precipitated phase consists of copper, aluminum, and magnesium elements, which is consistent with the results of the analysis of the selected electron diffraction pattern. And magnesium and copper elements are enriched at the interface, but iron and silicon elements are not enriched.

Combined with the above analyses, it can be seen that after the aging treatment of 1Ce-IQCp/6061 at  $170^\circ\text{C}$  with different holding times, the formed phases include the  $\beta$  phase, as well as the fine and diffusely distributed  $\text{Al}_2\text{CuMg}$  phase, and  $\beta''$  and  $\beta'$  phases. The aging precipitation sequence of the precipitated phases is as follows:  $\beta''$  phase ( $\text{Mg}_5\text{Si}_6$ )  $\rightarrow$   $\beta'$  phase ( $\text{Mg}_{1.8}\text{Si}$ ), in which the  $\beta''$  phase exhibits high co-lattice strain energy with the matrix, which can significantly improve the strength and hardness of 1Ce-IQCp/6061.



**Figure 8.** TEM characterization of  $\beta'$  and  $\beta''$  phases of 1Ce-IQCp/6061 after 10 h aging. (a) Bright-field image; (b,c) high-resolution and FFT of region 1 in Figure 8a; (d) high-resolution morphology and FFT of region 2 in Figure 8a.

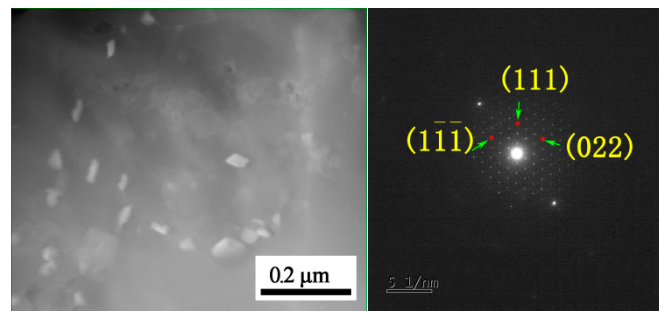


**Figure 9.** Bright-field image and the selected electron diffraction pattern of the  $\text{Al}_2\text{CuMg}$  phase of 1Ce-IQCp/6061 after aging for 10 h.

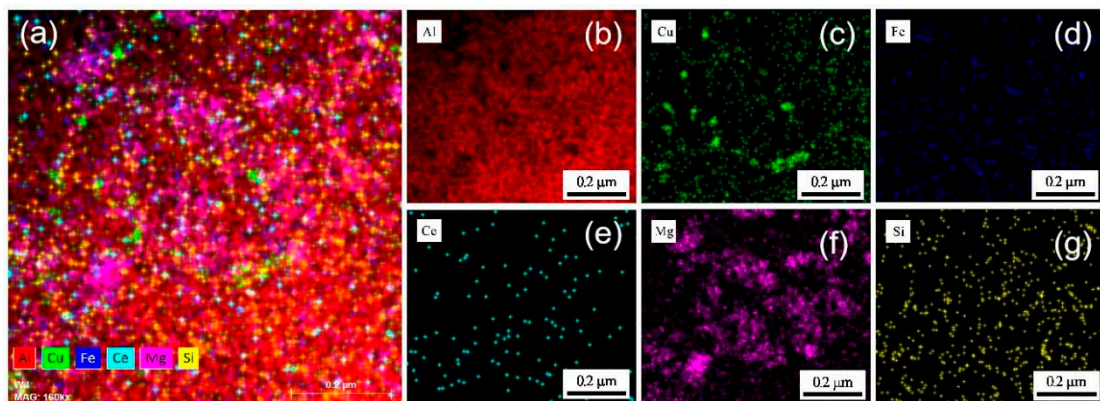


**Figure 10.** EDS surface scan analysis of 1Ce-IQCp/6061 aged for 10 h. (a) Full spectrum; (b) Al; (c) Cu; (d) Fe; (e) Ce; (f) Mg; (g) Si.

### 3.2. Effect of Aging Time on Hardness and Tensile Strength of 1Ce-IQCp/6061

The Vickers hardness and tensile strength of 1Ce-IQCp/6061 were tested after different aging times, and the results are shown in Figure 11. It can be seen that the Vickers hardness and tensile strength of 1Ce-IQCp/6061 both increase and then decrease with the increase in aging time and reach the maximum value when the aging time increases to 10 h. The results are shown in Figure 11.

As the aging time continues to increase, the Vickers hardness of the 1Ce-IQCp/6061 composites first decreases and then remains basically unchanged. The reason is that at the early stage of aging, the number of GP zones and the  $\beta''$  phase in the alloy gradually increases, and the precipitated phase is dominated by the  $\beta''$  phase. As the aging time continues to extend, the  $\beta''$  phase in the alloy is highly diffusely distributed, and the corresponding elastic stress reaches the maximum value, which has the strongest hindering effect on the dislocation.

And during the solid solution treatment process, the 1Ce-IQCp/6061 exhibits a rapid cooling rate, significant temperature range variation, and a large difference in the thermal expansion coefficient between the reinforcement and matrix. This leads to a significant thermal mismatch after the solid solution treatment, resulting in an increase in the dislocation density within the matrix. These high-density dislocations interact with the precipitated second phase during aging, enhancing the deformation resistance of the matrix and further improving the Vickers hardness and tensile strength of 1Ce-IQCp/6061. In the later stages of aging, the  $\beta'$  phase and other metastable phases form in the alloy. Simultaneously, these phases gradually grow and coarsen, resulting in a decreased impediment to dislocation motion, thus causing a slight reduction in the Vickers hardness and tensile strength of 1Ce-IQCp/6061.

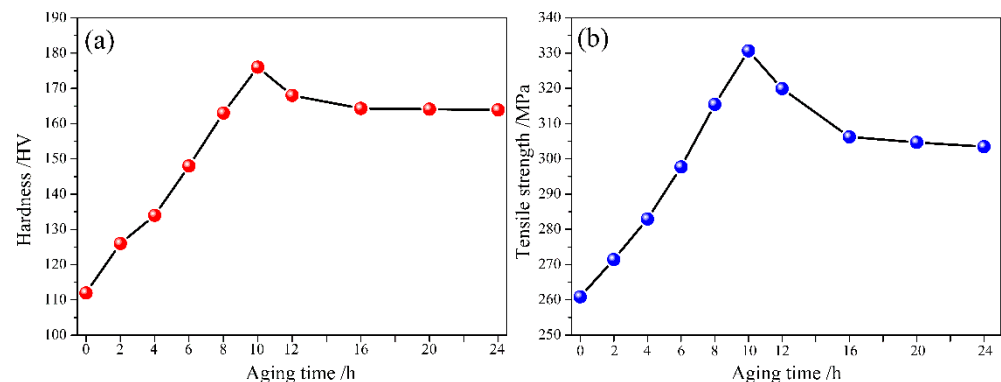


**Figure 11.** Effect of aging time on Vickers hardness and the tensile strength of 1Ce-IQCp/6061. (a) Vickers hardness; (b) tensile strength.

#### 4. Conclusions

The  $(Al_{63}Cu_{25}Fe_{12})_{99}Ce_1$  quasicrystalline particle-reinforced 6061 aluminum matrix composites were made by a vacuum hot pressing and sintering process, and a solid solution followed by the aging treatment was carried out to analyze the influences of aging time on the microstructure and mechanical properties of the composites. The conclusions are as follows:

- (1) It has been clarified that the optimum heat treatment process for  $(Al_{63}Cu_{25}Fe_{12})_{99}Ce_1$  quasicrystalline particle-reinforced 6061 aluminum matrix composites is a solid solution temperature of 530 °C, a holding time of 1 h, and water cooling, followed by an aging treatment with an aging temperature of 170 °C and a holding time of 10 h.
- (2) The phases of  $(Al_{63}Cu_{25}Fe_{12})_{99}Ce_1$  quasicrystalline particle-reinforced 6061 aluminum matrix composites after the aging treatment include the  $\beta$  phase, a small amount of the  $Al_2CuMg$  phase belonging to the orthorhombic crystalline system, as well as the  $\beta''$  phase and a small amount of the  $\beta'$  precipitated phase. The phases are meticulously and uniformly distributed, contributing to the strength and hardness of the 1Ce-IQCp/6061 alloy.
- (3) With the increase in aging time, the Vickers hardness and tensile strength of 1Ce-IQCp/6061 initially increase and then decrease, reaching their maximum value at 10 h of aging time.

**Author Contributions:** Conceptualization, J.W.; Methodology, J.W.; Software, J.W.; Formal analysis, J.W.; Investigation, J.W.; Resources, J.W.; Data curation, J.W.; Writing—original draft, J.W.; Writing—review & editing, J.W.; Supervision, Y.H. and Z.Y.; Project administration, J.W.; Funding acquisition, J.W. All authors have read and agreed to the published version of the manuscript.

**Funding:** The current work was funded by the HuZhou Vocational & Technical College Special Exploration Project Funds for High-level Talents under grant no. 2024TS04.

**Data Availability Statement:** Data are contained within the article.

**Conflicts of Interest:** The authors declare no conflict of interest.

#### References

1. Cui, Z.; Jiang, H.; Zhang, D.; Rong, L. Inhibiting of the negative natural aging effect in Al-Mg-Si alloys. *Mater. Sci. Eng. A* **2024**, *894*, 146196. [CrossRef]
2. Martins, P.S.; Drumond, R.M.; Silva, E.R.D.; Ba, E.C.T.; de Souza Lima, V.E.; Barbosa, J.W.; Fernandes, G.H.N.; Firpe, P.M. Evaluation of the drilling process in 6061-T6 Al-Mg-Si alloys using AISI M-35 diamond-like carbon coated high-speed steel drill. *Tribol. Int.* **2024**, *192*, 109250. [CrossRef]
3. Howard, R.H.; Gallagher, R.C.; Field, K.G. Mechanical performance of neutron-irradiated dissimilar transition joints of aluminum alloy 6061-T6 and 304l stainless steel. *J. Nucl. Mater.* **2018**, *508*, 348–353. [CrossRef]
4. Milagre, M.X.; Pereira, M.S.; Gomes, A.A.; Scapin, M.; Franco, M.; Yokaichiya, F.; Genezini, F.; Costa, I. Corrosion characterization of the 6061 Al-Mg-Si alloy in synthetic acid rain using neutron tomography. *Appl. Radiat. Isot.* **2022**, *184*, 110197. [CrossRef]

5. Sun, Y.; Wu, G. Preparation and characterization of Al-Mg-Si matrix composites reinforced with  $Ti_2(Al,Si)C$  solid solution. *Mater. Lett.* **2023**, *353*, 135266. [[CrossRef](#)]
6. Qi, Y.; Jia, L.; Ye, C.; Jin, Z.; Liu, Y.; Wang, W.; Zhang, H. Strengthening effects of gp zone induced by  $SiC_p$  size variations in Al-Si-Mg matrix composites. *J. Mater. Res. Technol.* **2023**, *27*, 7521–7531. [[CrossRef](#)]
7. Yi, R.; Chen, C.; Shi, C.; Li, Y.; Li, H.; Ma, Y. Research advances in residual thermal stress of ceramic/metal brazes. *Ceram. Int.* **2021**, *47*, 20807–20820. [[CrossRef](#)]
8. Wolf, W.; Bolfarini, C.; Kiminami, C.S.; Botta, W.J. Recent developments on fabrication of Al-matrix composites reinforced with quasicrystals: From metastable to conventional processing. *J. Mater. Res.* **2021**, *36*, 281–297. [[CrossRef](#)]
9. Schurack, F.; Eckert, J.; Schultz, L. Synthesis and mechanical properties of cast quasicrystal-reinforced Al-alloys. *Acta Mater.* **2001**, *49*, 1351–1361. [[CrossRef](#)]
10. Wolf, W.; Bolfarini, C.; Kiminami, C.S.; Botta, W.J. Designing new quasicrystalline compositions in Al-based alloys. *J. Alloys Compd.* **2020**, *823*, 153765. [[CrossRef](#)]
11. Wang, J.; Yang, Z.; Wang, L.; Li, J. Interfacial reaction kinetics of  $(Al_{63}Cu_{25}Fe_{12})_{99}Ce_1$  quasicrystal reinforced 6061 aluminum matrix composites. *J. Alloys Compd.* **2023**, *955*, 170261. [[CrossRef](#)]
12. Shadangi, Y.; Sharma, S.; Shivam, V.; Basu, J.; Chattopadhyay, K.; Majumdar, B.; Mukhopadhyay, N.K. Fabrication of Al-Cu-Fe quasicrystal reinforced 6082 aluminum matrix nanocomposites through mechanical milling and spark plasma sintering. *J. Alloys Compd.* **2020**, *828*, 154258. [[CrossRef](#)]
13. Wang, J.; Yang, Z.; Ma, Z.; Duan, H.; Zhang, J.; Tao, D.; Li, J. Effect of the addition of cerium on the microstructure evolution and thermal expansion properties of cast Al-Cu-Fe alloy. *Mater. Res. Express* **2021**, *8*, 36503. [[CrossRef](#)]
14. Silva, L.P.M.E.; Zepon, G.; Santos, A.J.; Câmara, M.A.; Kiminami, C.S.; Bolfarini, C.; Botta, W.J.; Wolf, W. A wear-resistant  $Al_{85}Cu_6Fe_3Cr_6$  spray-formed quasicrystalline composite. *Materialia* **2022**, *21*, 101367. [[CrossRef](#)]
15. de Araujo, A.P.M.; Kiminami, C.S.; Uhlenwinkel, V.; Gargarella, P. Processability of recycled quasicrystalline Al-Fe-Cr-Ti composites by selective laser melting—A statistical approach. *Materialia* **2022**, *22*, 101377. [[CrossRef](#)]
16. Yao, S.J.; Tang, Q.H.; Yang, J.; Wang, C.Y.; Sun, H.F.; Rong, R.L.; Sun, H.R.; Chu, G.N. Microstructural characterization and mechanical properties of 6061 aluminum alloy processed with short-time solid solution and aging treatment. *J. Alloys Compd.* **2023**, *960*, 170704. [[CrossRef](#)]
17. Kang, N.; Zhang, Y.; Mansori, M.E.; Lin, X. Laser powder bed fusion of a novel high strength quasicrystalline Al-Fe-Cr reinforced Al matrix composite. *Adv. Powder Mater.* **2023**, *2*, 100108. [[CrossRef](#)]
18. Farshidi, M.H.; Kazeminezhad, M.; Miyamoto, H. On the natural aging behavior of aluminum 6061 alloy after severe plastic deformation. *Mater. Sci. Eng. A* **2013**, *580*, 202–208. [[CrossRef](#)]
19. Prosviryakov, A.S.; Bazlov, A.I.; Mikhaylovskaya, A.V. Development of heat-resistant composites based on Al-Mg-Si alloy mechanically alloyed with aluminide particles. *JOM* **2024**, *76*, 1306–1318. [[CrossRef](#)]
20. Cui, C.Y.; Wan, T.Y.; Shu, Y.X.; Meng, S.; Cui, X.G.; Lu, J.Z.; Lu, Y.F. Microstructure evolution and mechanical properties of aging 6061 Al alloy via laser shock processing. *J. Alloys Compd.* **2019**, *803*, 1112–1118. [[CrossRef](#)]
21. Zang, A.; Khajezade, A.; Wang, X.; Parson, N.; Wells, M.; Poole, W.J. The spatial variation of crystallographic texture during axisymmetric solid bar extrusion of an Al-Mg-Si alloy. *Metall. Mater. Trans. A* **2024**, *55*, 1122–1136. [[CrossRef](#)]
22. Wang, J.; Yang, Z.; Duan, H.; Ma, Z.; Tao, D.; Li, J. Effect of heat treatment on microstructure and thermal expansion properties of as-cast  $(Al_{63}Cu_{25}Fe_{12})_{99}Ce_1$  alloy. *Met. Mater.* **2021**, *59*, 367–377. [[CrossRef](#)]
23. Yuan, W.; An, B. Effect of heat treatment on microstructure and mechanical property of extruded 7090/ $SiC_p$  composite. *Trans. Nonferrous Met. Soc. China* **2012**, *22*, 2080–2086. [[CrossRef](#)]
24. Yang, W.; Wang, M.; Zhang, R.; Zhang, Q.; Sheng, X. The diffraction patterns from  $\beta''$  precipitates in 12 orientations in Al-Mg-Si alloy. *Scr. Mater.* **2010**, *62*, 705–708. [[CrossRef](#)]
25. Vissers, R.; van Huis, M.A.; Jansen, J.; Zandbergen, H.W.; Marioara, C.D.; Andersen, S.J. The crystal structure of the  $\beta'$  phase in Al-Mg-Si alloys. *Acta Mater.* **2007**, *55*, 3815–3823. [[CrossRef](#)]
26. Zi, Y.; Zeqin, L.; Leyvraz, D.; Banhart, J. Effect of pre-ageing on natural secondary ageing and paint bake hardening in Al-Mg-Si alloys. *Materialia* **2019**, *7*, 100413. [[CrossRef](#)]

**Disclaimer/Publisher's Note:** The statements, opinions and data contained in all publications are solely those of the individual author(s) and contributor(s) and not of MDPI and/or the editor(s). MDPI and/or the editor(s) disclaim responsibility for any injury to people or property resulting from any ideas, methods, instructions or products referred to in the content.